PAPER Nr. : 27

STUDY OF ROTOR GUST RESPONSE BY MEANS OF THE LOCAL MOMENTUM THEORY

by

Akira Azuma, Professor
and
Shigeru Saito, Graduate Student
University of Tokyo
Tokyo, Japan

FIFTH EUROPEAN ROTORCRAFT AND POWERED LIFT AIRCRAFT FORUM
SEPTEMBER 4 – 7TH 1979 - AMSTERDAM, THE NETHERLANDS

STUDY OF ROTOR GUST RESPONSE BY MEANS OF THE LOCAL MOMENTUM THEORY

By

Akira Azuma and Shigeru Saito
University of Tokyo

SUMMARY

The vertical gust response for helicopter rotor in cruising flight is studied analytically by means of the local momentum theory (LMT) and experimentally in wind tunnel installing gust generator. By introducing the unsteady aerodynamic effects into the LMT and by taking the elastic deformation into the rotor blade, the vibratory characteristics of the flapping behaviour and the rotor forces can be obtained.

Since the LMT is possible to calculate the instantaneous load distribution along the rotor blade in desirable azimuthal or timewise interval, the effects of gradual penetration of the rotor into the gust can be studied and the Fourier analysis or power spectrum analysis of the rotor response can be applied to any kind of gust input.

Some results obtained analytically are verified by the experimental tests performed in the wind tunnel which generates step, sinusoidal and random vertical gusts by the motion of a series of cascaded vanes in the upstream of the flow.

1. Introduction

The helicopter rotor response due to vertical gusts has been treated in many ways theoretically and experimentally.[1~5] The variety of the analyses can be seen in the setting of the following assumptions: quasi-steady or unsteady aerodynamics, constant or variable induced velocity distribution, rigid or flexible blade, with or without hub motion, sudden or gradual penetration into the gust, and so on.

Since the rotor blade is operating in the unsteady flow field including the periodic variation of the horizontal or tangential velocity component as well as the vertical velocity component, the unsteady aerodynamic effect must be introduced in the calculation of the airloading of a blade element working with high reduced frequency.

The LMT has been developed[6~8] to obtain the instantaneous airloading acting on the rotor blade and the related downwash distribution on the rotor operating plane in a reasonable range of accuracy. The theory can evaluate the effect of the tip vortices trailed from the preceding blades by introducing the attenuation coefficient which expresses the degeneration of the induced velocity at a local station on the rotor operating plane after the blade element having passed on that station.

The idea can easily be applied to the gust response of the rotor blade by taking the vertical velocity component of the gust into the normal velocity component of the airflow at the blade element. This enable us to calculate the aeroelastic characteristics and the flapping behaviour of the rotor blades penetrating gradually into any kind of gust shapes. Then the obtained thrust, for example, shows very vibratory characteristics which have not be seen in any other paper, and thus the Fourier analysis will be introduced for the random gust.

The hub motion can also be introduced to the LMT by only adjusting the velocity components at the blade element by those given as the vector summation of the hub motion and the flapping motion.

The wind tunnel test can validate the theory even in a restricted condition that the rotor is bounded in a narrow test area and its hub is fixed to a point in that area without having any degree of freedom in motion except the rotor revolution.

2. Rotor response for step and sinusoidal gusts

Let us consider the following two types of spatially frozen gust:

$$\text{Step:}\quad w_G(X,t) = \begin{cases} 0 & t<t_0 \\ w_{G_0} & t\geq t_0 \end{cases} \tag{1}$$

$$\text{Sinusoidal:}\quad w_G(X,t)=w_{G_0}\sin\kappa(X+X_0-V_G t), \tag{2}$$

where the coordinate system can be seen in Fig. 1. The transformation of the velocity components into the blade coordinates axes will be given in APPENDIX A. Then, following to the LMT yields

$$\begin{aligned} \gamma_i &= \int_{x_i}^{x_{i+1}} \{\tfrac{1}{2}\rho V_i^2 c_i a(\theta_i-\phi_i)-\rho\pi(c_i/2)^2\dot{V}_N\}dx/(x_{i+1}-x_i) \\ &= \int_{x_i}^{x_{i+1}} \sum_{\nu=1}^{i}\{4L_\nu/\pi R(1-x_\nu)\}\{R\Omega(\mu\sin\psi+x)/V_{\nu,c}\}\sqrt{1-\{(2x-1-x_\nu)} \\ &\qquad \overline{/(1-x_\nu)\}^2}\,dx/(x_{i+1}-x_i) \end{aligned} \tag{3}$$

where

$$\begin{aligned} L_\nu &= 2\rho S_\nu V_{\nu,c}(v_{\nu jk}-v_{\nu-1\,jk})+M_\nu(\dot{v}_{\nu jk}-\dot{v}_{\nu-1\,jk}) \\ V_i &= V\sin(\psi_0+k2\pi/b+\textstyle\sum_{\nu=0}^{j-1}\nu\Delta\psi)+R\Omega(x_i+x_{i+1})/2 \\ V_{\nu,c} &= R\Omega(\psi_0+k2\pi/b+\textstyle\sum_{\nu=0}^{j-1}\nu\Delta\psi)+R\Omega(1+x_\nu)/2 \\ S_\nu &= \pi\{R(1-x_\nu)/2\}^2, \quad c_i = c[x=(x_i+x_{i+1})/2] \\ \theta_i &= \theta[x=(x_i+x_{i+1})/2] \\ M_\nu &= \tfrac{4}{3}\rho\pi ab/\int_0^{\pi/2}\sqrt{(a/b)^2\sin^2\theta+\cos^2\theta}\,d\theta \end{aligned} \tag{4}$$

$$a = (R/2)(1-x_v), \quad b = c_i/2$$

$$\phi_i = (V_N+v^j_{\ell m}+v_{ijk})/V_i$$

$$V_N = V\sin i+V\cos i\cdot\beta\cos\psi+R(x-x_\beta)\dot{\beta} - w_G$$

$$v^i_{\ell m} = c^{j-1}_{\ell m}(v^{j-1}_{\ell m}+\sum_{i=\ell}^{n}\sum_{k=\ell}^{b} v_{i\ j-1\ k}\cdot\delta_{\ell m}).$$

The equations of motion for vertical acceleration and the flapping motion for articulated blades can be given respectively by

$$\ddot{z}/g = T/W-1 \tag{5}$$

$$I\ddot{\beta}+M_\beta\Omega^2\beta = \int_{r_\beta}^{R}(f_a-f_g)(r-r_\beta)dr \tag{6}$$

where

$$T = \sum_{k=0}^{b-1}\{\sum_{i=1}^{n}\ell_i-m_\beta(\ddot{z}+r_{cG}\ddot{\beta})\}$$

$$I = \int_{r_\beta}^{R}(r-r_\beta)^2dm$$

$$M_\beta = \int_{r_\beta}^{R}r(r-r_\beta)dm$$

$$f_g = g\cos\Theta dm$$

$$f_a = \frac{1}{2}\rho(R\Omega)^2ac(K_\theta\theta-K_{W_G}U_P/U_T) \tag{7}$$

$$r_{cG} = \int_{r_\beta}^{R}rdm/\int_{r_\beta}^{r}dm$$

$$U_P = -R\Omega\{\mu\tan i+\beta\mu\cos\psi+v^j_{\ell m}/R\Omega-w_G/R\Omega+(\dot{\beta}/\Omega)(x-x_\beta)\}$$

$$U_T = R\Omega(x+\mu\sin\psi)$$

$$\mu = V\cos i/R\Omega,$$

and where the lift defficiency function, K_θ and K_{w_G}, showing the unsteady effects of the pitching motion of the blade and of the vertical gust, can be seen in APPENDIX B.

Fig. 2 and Fig. 3 show the time responses of load factor T/W, flapping angle β and tip path plane (β_{1c}, β_{1s}) of a rotor penetrating gradually into a step gust and a sinusoidal gust respectively. In these examples of calculation it has been assumed that the blade is affected by the quasi-steady aerodynamic force and the rotor hub is either fixed (dotted line) or free for only heaving motion (solid line).

The vibratory characteristics of the load factor is obvious. For the step gust two peaks and one valley are observed in the flapping angle as well as the load factor before the response attains to the steady state.

The first peak appears with time delay of 0.23 sec. that is equivalent to the duration within which the rotor has fully bathed in the gust or $R/V\cos i = 1/\mu\Omega$. The valley is resulted from the downwash flow caused by the upward flapping. Then the response tends to recover the steady state with the inherent or natural frequency of the blade flapping motion, which is nearly equal to the undamped natural frequency, $(M_\beta/I)\Omega \cong \Omega$.

The inertial effect of the flapping motion brings the similar fluctuation in the load factor with the phase lag of π. Due to the gradual penetration of the rotor into the upward gust the rotor tends to tilt backward initially, then rightward, and finally falls into a terminal orbit.

Similar results can be seen in the response for the sinusoidal gust too. However, the initial rise in the response of the load factor and the flapping angle are more gradual than those obtained for the step gust, because of the moderate slope of the sine function. This is also verified by seeing Fig. 4 which shows the difference in thrust responses between the sudden and the gradual penetrations of the rotor into a step gust.

Allowing the heaving motion of the hub does not change the peak values appreciably but alleviates the load factor as well as the flapping angle in the terminal state for the step gust.

It is, from the theoretical consideration described in APPENDIX A, obvious that for the sinusoidal gust the response is, in either load factor or the flapping angle, comprised of three fundamental harmonic components, the angular velocities of which are ω_G and $\omega_G \pm \Omega$ respectively, as shown in Fig. 5.

3. Wind tunnel test of a model rotor

Wind tunnel experiments were conducted at National Aerospace Laboratory (NAL), using a model rotor subjected to vertical gust. An overall view of the model rotor and mount set up in the wind tunnel is shown in Fig. 6. A series of vanes which generates the vertical gust in any shape within the frequency of 20 Hz can be seen at the backside of the model rotor. Mechanical properties of the model rotor are also given in Fig. 6.

Shown in Fig. 7 is a systematic arrangement of the instruments for measuring forces, moments, angular velocities, and angles; the rotor driving system; and the filtering, monitoring, and recording systems.

Two examples of test results for the step and the sinusoidal gusts are shown in Fig. 8 and 9 respectively. The vibratory characteristics were amplified by uneven finish of the blades and the lack of rigidity of the model support system.

Fig. 10 and 11 show comparisons of thrust between the theoretical and experimental results at the initial stage for the step and sinusoidal gusts respectively. It can be seen that the satisfactory results were obtained. In order to stress the above fact there are prepared two drawings, Fig. 12 and 13. The former shows the time lags of the first peak of thrust responses for the step gust of (a) upwind and (b) downwind respectively. Except a misterious case at $\mu=0.15$ for the upwind, the theoretical results show good coincidence with the experimental data. The latter shows the power spectrum of the thrust coefficient for a sinusoidal gust with angular frequency of which is $\omega_G = 25.1$ rad/sec. The biggest peak at Ω was resulted from the mechanical vibration of the overall rotor systems. Shown in Fig. 14 are comparison between the computed and experimental results on the deviation of the (a) thrust coefficient and (b) flapping angle from their mean values.

4. Refinement of the analyses

Three important factors which are supposed to give some effects on the gust response, (a) Lock number, (b) blade flexibility, and (c) unsteady aerodynamics, are treated here for the refinement of the analyses.

(a) Lock Number

Fig. 15 shows the theoretical comparison of time responses of the load factor for the step gust in three different Lock numbers, $\gamma=4.42$, 8.84 and 17.68. As expected intuitively, any noticeable change is not observed except that the larger Lock number has better damping.

(b) Blade Elasticity

The blade bending flexibility can easily be introduced to the dynamic analyses based on the LMT. The flapwise and chordwise bending and torsional deflections were expressed in modal expansion series and solved by Holzer-Myklestad method[9,10].

The followings are the correction terms in blade pitch and velocities due to the blade deflections:

$$\Delta\theta = \phi$$

$$\Delta U_P = \dot{w} \qquad (8)$$

$$\Delta U_T = \dot{v}$$

The equations of blade deflections can be seen in APPENDIX C.

Shown in Fig. 16 a and b are the time responses of load factor of the rotor penetrating gradually into (a) step gust and (b) sinusoidal gust respectively. The rotor blades are considered to be either flexible, shown by solid lines, or rigid, shown by dotted lines. It can be seen that the bending flexibility of the blade delays the response and attenuates the load factor. The difference is appreciable for the sinusoidal gust, specifically, in steady response.

(c) Unsteady Aerodynamics

As written in APPENDIX B, the unsteady lift of a two-dimensional wing which has a simusoidal pitching and surging motions and is operationg in a sinusoidal gust can be obtained analytically. The principal parts of K_Θ and $K_{\overline{W}_G}$ in APPENDIX B can be approximated by the following complex expressions, lift defficiency functions for complex sinusoidal inputs, in the small reduced frequency k :

$$K_\Theta \cong J_0(ka_2)C(k)e^{-j(ka_2\cos\psi)}$$
$$K_{\overline{W}_G} \cong J_0(ka_2)S(k)e^{-j(ka_2\cos\psi-k)} \qquad (9)$$

where C(k) and S(k) are the theodorsen and Sears functions respectively and $J_0(ka_2)$ is the 0-th order Bessel function.

The above lift defficiency functions, K_Θ and $K_{\overline{W}_G}$, are respectively shown in Fig.17 a and b, in comparison with the Theodorsen and Sears functions. As seen from equations(9) and these figures the lift difficiency functions are very close to the original functions, C(k) and S(k).

Shown in Fig.18 is time responses of the load factor for a sinusoidal gust in comparison of the unsteady aerodynamics with the quasi-steady aerodynamics. A little phase difference can be visible but the dynamic behaviour is almost same for the both results because of small reduced frequency. However, higher reduced frequency does not bring any appreciable thrust change because the wave lengh of the gust approaches to the rotor diameter.

5. Conclusion

The local momentum theory(LMT) has been applied to analyze the gust response of helicopter rotor and verified by the wind tunnel tests.

Since the LMT is possible to calculate the instantaneous load distribution along the rotor blade in desirable timewise interval, the effects of gradual penetration of the rotor into the gust can be studied and the Fourier analysis can be well applied to the random gusts.

The blade flexibility was an important factor for determining the flapping behaviour of the rotor blade in the vertical gust, whereas the unsteady aerofynamics of the rotor blade did not bring any appreciabe change from the quasi-steady aerodynamics because the reduced frequency in the sinusoidal gust was considered to be small.

Nomenclature

a	= lift slope	l	= airloading
b	= wing semi-chord and blade number	m	= blade section mass
C, C_{lm}^{j}	= attenuation coefficients	n	= load factor
$C(k)$	= Theodorsen function	r	= radius
C_{d_0}	= airfoil profile drag coefficient	$S(k)$	= Sears function
C_T	= thrust coefficient = $T/\rho\pi R^2(R\Omega)^2$	T	= thrust and tension
c	= wing chord	t	= time
E	= Young's modulus	U_T, U_P	= tangential and normal components of velocity at a blade element
e	= distance between mass and elastic axis		
e_0	= distance at root between elastic axis and feathering axis	V	= forward velocity
		V_G	= gust forward velocity
G	= shear modulus	v_G	= vertical gust velocity
g	= gravity acceleration	v_{G_0}	= gust amplitude
I_x, I_y	= blade cross-section moment of inertia	β	= flapping angle = $\beta_0 + \beta_{1c}\cos\psi + \beta_{1s}\sin\psi$
i	= inclination angle of tip-path-plane	γ	= Lock number = $\rho acR^4/I$
J	= torsional rigidity constant	δ	= δ function
$J_n(z)$	= Bessel function of n-th order	θ	= pitch angle of a body
j	= imaginary = $\sqrt{-1}$	κ	= wave number = $2\pi/\lambda$
K_{w_G}	= unsteady attenuate coefficient for vertical gust	λ	= wave length
		ρ	= air density
K_θ	= unsteady attenuate coefficient for pitching motion of a blade	$\phi(s)$	= Wagner function
		$\Psi(s)$	= Kussner function
k	= reduced frequency	ψ	= azimuth angle
k_A	= blade cross-section polar radius of gyration	ψ_0	= initial azimuth angle
		ω_G	= angular velocity of a gust

APPENDIX A Expression of sinusoidal gust in the rotor cordinate system

Let us assume that the rotor advances diagonally with the yawing angle, Ψ, to a two-dimensional-sinusoidal gust. The gust given by equation (2) can be expressed in the rotor coordinate system by applying the successive coordinate transformations such as

(i) transformation from the hub coordinate axes to the stationary coordinate axes

$$T_1 = \begin{pmatrix} \cos\Psi & \sin\Psi & 0 \\ -\sin\Psi & \cos\Psi & 0 \\ 0 & 0 & 1 \end{pmatrix}, \qquad \text{(A-1)}$$

(ii) transformation from the rotor coordinate axes and the hub coordinate axes,

$$T_2 = \begin{pmatrix} \cos(\Omega t+\psi_0) & -\sin(\Omega t+\psi_0) & 0 \\ \sin(\Omega t+\psi_0) & \cos(\Omega t+\psi_0) & 0 \\ 0 & 0 & 1 \end{pmatrix}. \qquad \text{(A-2)}$$

Then, a point along X_R axis, r, is expressed in the (X,Y,Z) axes as follows:

$$(X,Y,Z)^T = T_1 \cdot T_2 \cdot (r,0,0)^T + T_1 \cdot (-Vt,0,0)^T + (X_0,Y_0,Z_0)^T, \quad \text{(A-3)}$$

where the detailed expression of the X is given by

$$X = r\cos(\Omega t+\psi_0-\Psi) - Vt\cos\Psi + X_0. \qquad \text{(A-4)}$$

Substituting this into equation (2) yields

$$\begin{aligned} w_G(r,t)/w_{G_0} &= \sin[\kappa\{r\cos(\Omega t+\psi_0-\Psi)-(V\cos\Psi+V_G)t+x_0\}] \\ &= \cos(w_G t+\phi_1)[2J_0(a_s)J_1(a_c)\cos\Omega t \\ &+2\sum_{n=1}^{\infty}\{2J_1(a_c)J_{2n}(a_s)\cos(\Omega t)\cos(2n\Omega t)+(-1)^n \\ &J_0(a_s)J_{2n+1}(a_c)\cos(2n+1)\Omega t\}+4\sum_{n=1}^{\infty}\{(-1)^n J_{2n+1}(a_c) \\ &\cos(2n+1)\Omega t\cdot\sum_{m=1}^{\infty}J_{2m}(a_s)\cos(2m\Omega t)\}-2J_0(a_c)J_1(a_s) \\ &\sin(\Omega t)-2\sum_{n=1}^{\infty}\{J_0(a_c)J_{2n+1}(a_s)\sin(2n+1)\Omega t+(-1)^n \\ &2J_1(a_s)J_{2n}(a_c)\sin(\Omega t)\cos(2n\Omega t)\}-4\sum_{n=1}^{\infty}\{(-1)^n J_{2n}(a_c) \\ &\cos(2n\Omega t)\cdot\sum_{m=1}^{\infty}J_{2m+1}(a_s)\sin(2m+1)\Omega t\}]+\sin(w_G t+\phi_1) \\ &[J_0(a_c)J_0(a_s)+2\sum_{n=1}^{\infty}\{J_0(a_c)J_{2n}(a_s)+(-1)^n J_0(a_s)J_{2n} \\ &(a_c)\}\cos(2n\Omega t)+4\sum_{n=1}^{\infty}\{(-1)^n J_{2n}(a_c)\cos(2n\Omega t)\cdot \end{aligned}$$

$$\sum_{m=1}^{\infty} J_{2m}(a_s)\cos 2(m\Omega t)\}+2J_1(a_c)J_1(a_s)\sin 2\Omega t$$
$$+4\sum_{n=1}^{\infty}\{J_1(a_c)J_{2n+1}(a_s)\cos(\Omega t)\sin(2n+1)\Omega t+(-1)^n J_1$$
$$(a_s)J_{2n+1}(a_c)\sin(\Omega t)\cos(2n+1)\Omega t+(-1)^n J_{2n+1}(a_c)$$
$$\cos(2n+1)\Omega t\cdot\sum_{m=1}^{\infty} J_{2m+1}(a_s)\sin(2m+1)\Omega t\}] \qquad (A\text{-}5)$$

where

$$a_c = a(x)\cos\psi_1$$
$$a_s = a(x)\sin\psi_1$$
$$a(x) = \kappa Rx = \kappa r \qquad (A\text{-}6)$$
$$\psi_1 = \psi_0 - \Psi$$
$$\phi_1 = x_0\kappa$$

APPENDIX B Unsteady aerodynamics for rotor blade

When a rotor blade is operating in a vertical gust, the quasi-steady airloading can be given by

$$l_{qs} = \frac{1}{2}\rho ac(U_T^2\theta + U_T w_G) \qquad (B\text{-}1)$$

where

$$U_T = R\Omega(x+\mu\sin\Omega t). \qquad (B\text{-}2)$$

However, if the variations of the blade pitch and the gust are not slow, the unsteady aerodynamic loading must be considered. Then, by applying Duhamel's integration after having multiplied the time derivatives of Wagner function Φ for the pitch change and the Küssner function Ψ for the gust variation, the following unsteady airloading can be obtained.

$$l_{us} = -\frac{1}{2}\rho ac\int_{-\infty}^{t}\{U_T^2\theta\frac{d}{d\tau}\Phi(s)+U_T w_G\frac{d}{d\tau}\Psi(s)\}d\tau \qquad (B\text{-}3)$$

where

$$\Phi(s) = \frac{1}{2\pi}\int_{-\infty}^{\infty}\frac{C(k)}{jk}e^{jks}dk$$
$$\Psi(s) = \frac{1}{2\pi}\int_{-\infty}^{\infty}\frac{S(k)}{jk}e^{jk(s-1)}dk \qquad (B\text{-}4)$$
$$s = s(\tau,t) = \frac{1}{b}\int_{\tau}^{t}U_T(\tau)d\tau = \left(\frac{R}{b}\right)\{\Omega x(t-\tau)-\mu(\cos\Omega t-\cos\Omega\tau)\}$$

and where $C(k)$ and $S(k)$ are Theodorsen and Sears functions respectively[11].

By considering the first harmonic feathering oscillation,

$$\theta = \theta_0 + \theta_{1c}\cos\psi + \theta_{1s}\sin\psi, \qquad \text{(B-5)}$$

and a random gust written in Fourier expansion series,

$$w_G(t) = w_{G_0} + \sum_{m=1}^{\infty} (w_{G,mc}\cos\omega_m t + w_{G,ms}\sin\omega_m t) \qquad \text{(B-6)}$$

equation (B-3) yields

$$\gamma_{us}/\tfrac{1}{2}\rho(R\Omega)^2 ac = K_\theta\cdot\Theta + K_{w_G}\cdot(w_G/U_T) = K_\theta\cdot\Theta + K_{\overline{W}_G}\cdot\overline{W}_G \qquad \text{(B-7)}$$

The detailed expression of the above equation can be seen in Table B-1.

APPENDIX C Modal equations of motion

Equations of blade chordwise and flapwise bending deflections, v and w, and torsional deflection, ϕ, can be given respectively by the following equations[12]:

$$-(Tv')' + [\{EI_z - (EI_z - EI_y)\sin^2\theta\}v'' - (EI_z - EI_y)\{\tfrac{1}{2}w''\sin 2\theta - \phi v''\sin 2\theta + \phi w''\cos 2\theta\}]'' = L_v \qquad \text{(C-1)}$$

$$-(Tw')' + [\{EI_y + (EI_z - EI_y)\sin^2\theta\}w'' + (EI_z - EI_y)\{\tfrac{1}{2}v''\sin 2\theta + \phi v''\cos 2\theta + \phi w''\sin 2\theta\}]'' = L_w \qquad \text{(C-2)}$$

$$-[(GJ + Tk_A^2\phi')]' + (EI_z - EI_y)[\tfrac{1}{2}\{(w'')^2 - (v'')^2\}\sin 2\theta + v''w''\cos 2\theta] = M_\phi \qquad \text{(C-3)}$$

where

$$\begin{aligned} L_v &= F_{ay} + m[-2\Omega\dot{u} + 2e\Omega(\dot{v}' + \theta\dot{w}') + e\theta\ddot{\theta} \\ &\quad + \Omega^2(e_0 + 2e)] - m[\ddot{v} - e\theta\ddot{\phi} - \Omega^2(v - e\theta\phi)] \\ L_w &= F_{az} - m(q + e\ddot{\theta} - e\Omega^2\theta) - m(\ddot{w} + e\ddot{\phi}) \\ M_\phi &= M_{ax} - m[eg + k_A^2(\ddot{\theta} + \Omega^2\theta + 2\Omega\theta\dot{v}') + e\theta(e_0\Omega^2 - 2\Omega\dot{u})] \\ &\quad - me[\ddot{w} - \theta\ddot{v} + \theta\Omega^2 v + e_0\Omega^2\phi + r\Omega^2(w' - \theta v')] \end{aligned} \qquad \text{(C-4)}$$

and where

$$(\dot{}) = \frac{d}{dt}(\ ) \qquad ( )' = \frac{d}{dr}(\ ) \qquad \text{(C-5)}$$

$$F_{ay} = \frac{1}{2}\rho U_T^2 c C_{d_0} + \ell_i \phi_i$$

$$F_{az} = \ell_i \text{ (see eq.(3))} \qquad \text{(C-6)}$$

$$M_\phi = \frac{1}{2}\rho U_T^2 c^2 C_m$$

REFERENCES

1) Harvey, K. W., Blankenship, B. L. and Drees, J. M. : Analytical Study of Helicopter Gust Response at High Forward Speeds. USAAVLABS Technical Report 69-1, AD862594, September 1969.

2) Bergquist, Russell R. : Helicopter Gust Response Including Unsteady Aerodynamic Stall Effects. USAAMRDL Technical Report 72-68, AD763957, May 1973.

3) Judd, M. and Newman, S. J. : An Analysis of Helicopter Rotor Response due to Gusts and Turbulence. Vertica, Vol. 1, 1977, pp.179-188.

4) Yasue, Masahiro, Vehlow, Charles A., and Ham, Norman D. : Gust Response and Its Alleviation for a Hingeless Helicopter Rotor in Cruising Flight. Paper No. 28, Fourth European Rotorcraft and Powered Lift Aircraft Forum, September 13-15, 1978.

5) Dahl, H. J. and Faulkner, A. J. : Helicopter Simulation in Atmospheric Turbulence. Paper No. 29, Fourth European Rotorcraft and Powered Lift Aircraft Forum, September 13-15, 1978.

6) Azuma, Akira and Kawachi, Keiji : Local Momentum Theory and Its Application to the Rotary Wing. Journal of Aircraft, Vol. 16, No. 1, January 1979, Page 6-14.

7) Nakamura, Yoshiya and Azuma, Akira : Rotational Noise of Helicopter Rotor. To be published in VERTICA.

8) Azuma, Akira, Saito, Shigeru, Kawachi, Keiji, and Karasudani, Takahisa : Application of the Local Momentum Theory to the Aerodynamic Characteristics of Tandem Rotor in Yawed Flight. Paper No. 4, Fourth European Rotorcraft and Powered Lift Aircraft Forum, September 13-15, 1978.

9) Myklestad, N. O. : Fundamentals of Vibration Analysis. McGraw-Hill Book Company, Inc., New York, 1944.

10) Isakson, G. and Eisley, J. G. : Natural Frequencies in Coupled Bending and Torsion of Twisted Rotating and Nonrotating Blades. NASA CR-65, July 1964.

11) Bisplinghoff, R. L., Ashley, H. and Halfman, R. L. : Aeroelasticity. Addison-Wesley Publishing Company, Inc. Reading, Mass. 1955.

12) Hodges, D. H., Ormiston, R. A. and USAARDL : Stability of Elastic Bending and Torsion of Uniform Cantilever Rotor Blades in Hover With Variable Structural Coupling. NASA TN D-8192, April 1976.

TABLE 1 Rotor dimensions

Item		Rotor used in theoretical calculation	Roter used in experimental test
Rotor radius,	R	8.53 m	0.75 m
No. of blades,	b	4	2
Blade chord,	c	0.417 m	0.085 m
Rotor rotational speed,	Ω	23.67 rad./sec.	104.7 rad./sec.
Blade twist angle,	θ_t	-8 deg.	0 deg.
Collective pitch angle,	θ_0	8 deg.	2 ~ 6 deg.
Cyclic pitch angle,	θ_{1c} θ_{1s}	0 deg. 0 deg.	-6 ~ 6 deg. -6 ~ 6 deg.
Position of flapping hinge,	r_β	0.3 m	0.03 m
Blade cut off,	r_c	0.594 m	0.086 m
C. G. position of blade,	r_{cG}	2.74 m	0.2475 m
Blade mass,	m_β	10.86 kg sec.^{2} m^{-1}	0.058 kg sec.^{2} m^{-1}
Moment of inertia of blade,	I	162.6 kg m sec.^{2}	0.0125 kg m sec.^{2}
Mass moment of blade,	M_β	169.3 kg m sec.^{2}	0.01638 kg m sec.^{2}
Lock number,	γ	8.84	1.45
Wing section		NACA 0012	NACA 0012
Advance ratio,	μ	0.18	0.15 ~ 0.3
Gross weight,	W	6,353 kg	———

Table 2

$$l_{un}/\tfrac{1}{2}\rho(R\Omega)^2 nc = K_{\theta}\cdot\theta + K_{w_G}\cdot w_G/U_T$$

$$= (k_{\theta_0}, K_{\theta_{1c}}, K_{\theta_{1s}})\cdot(\theta_0, \theta_{1c}, \theta_{1s})^T + (K_{w_{G_0}}, K_{w_{G_{1c}}}, K_{w_{G_{1s}}}, \ldots)\cdot(w_{G_0}, w_{G_{1c}}, w_{G_{1s}}, \ldots)^T$$

$$= K_{\theta}\cdot\theta + K_{\bar{w}_G}\cdot\bar{w}_G$$

$$= (K_{\theta_0}, K_{\theta_{1c}}, K_{\theta_{1s}}, K_{\theta_{2c}}, K_{\theta_{2s}}, K_{\theta_{3c}}, K_{\theta_{3s}})\cdot(\theta_0, \theta_{1c}, \theta_{1s}, \theta_{2c}, \theta_{2s}, \theta_{3c}, \theta_{3s})^T + (K_{\bar{w}_{G,0,1}}, K_{\bar{w}_{G,0,2}}, K_{\bar{w}_{G,1c,1}}, K_{\bar{w}_{G,1c,2}}, K_{\bar{w}_{G,1c,3}}, K_{\bar{w}_{G,1s,1}}, K_{\bar{w}_{G,1s,2}}, K_{\bar{w}_{G,1s,3}}, K_{\bar{w}_{G,2c,1}}, \ldots)\cdot(\bar{w}_{G_{0,1}}, \bar{w}_{G_{0,2}}, \bar{w}_{G_{1c,1}}, \bar{w}_{G_{1c,2}}, \bar{w}_{G_{1c,3}}, \ldots)^T$$

$$K_{\theta_0} = 1$$

$$K_{\theta_{1c}} = f_c(\mu,\Omega,t) - g_c(\mu,\Omega,t) - F_c(\mu,\Omega,t)_{n=odd} + F_c(\mu,\Omega,t)_{n=even})$$

$$K_{\theta_{1s}} = f_s(\mu,\Omega,t) + g_s(\mu,\Omega,t) + F_s(\mu,\Omega,t)_{n=odd} + F_s(\mu,\Omega,t)_{n=even})$$

$$K_{\theta_{2c}} = f_c(\mu,2\Omega,t) - g_c(\mu,\Omega,t) - F_c(\mu,2\Omega,t)_{n=odd} + F_c(\mu,2\Omega,t)_{n=even})$$

$$K_{\theta_{2s}} = f_s(\mu,2\Omega,t) + g_s(\mu,\Omega,t) + F_s(\mu,2\Omega,t)_{n=odd} + F_s(\mu,2\Omega,t)_{n=even})$$

$$K_{\theta_{3c}} = f_c(\mu,3\Omega,t) - g_c(\mu,3\Omega,t) - F_c(\mu,3\Omega,t)_{n=odd} + F_c(\mu,3\Omega,t)_{n=even})$$

$$K_{\theta_{3s}} = f_s(\mu,3\Omega,t) + g_s(\mu,3\Omega,t) + F_s(\mu,3\Omega,t)_{n=odd} + F_s(\mu,3\Omega,t)_{n=even}+$$

$$K_{\bar{w}_{G_{0,1}}} = 1$$

$$K_{\bar{w}_{G_{0,2}}} = f_{s,G}(\mu,\Omega,t) + g_{s,G}(\mu,\Omega,t) + F_{s,G}(\mu,\Omega,t)_{n=odd} + F_{s,G}(\mu,\Omega,t)_{n=even})$$

$$K_{\bar{w}_{G,mc,1}} = f_{c,G}(\mu,\omega_{m_1},t) - g_{c,G}(\mu,\omega_{m_1},t) + F_{c,G}(\mu,\omega_{m_1},t)_{n=odd} + F_{c,G}(\mu,\omega_{m_1},t)_{n=even})$$

$$K_{\bar{w}_{G,mc,2}} = f_{c,G}(\mu,\omega_{m_2},t) - g_{c,G}(\mu,\omega_{m_2},t) - F_{c,G}(\mu,\omega_{m_2},t)_{n=odd} + F_{c,G}(\mu,\omega_{m_2},t)_{n=even})$$

$$K_{\bar{w}_{G,mc,3}} = f_{c,G}(\mu,\omega_{m_3},t) - g_{c,G}(\mu,\omega_{m_3},t) - F_{c,G}(\mu,\omega_{m_3},t)_{n=odd} + F_{c,G}(\mu,\omega_{m_3},t)_{n=even})$$

$$K_{\bar{w}_{G,ms,1}} = f_{s,G}(\mu,\omega_{m_1},t) + g_{s,G}(\mu,\omega_{m_1},t) + F_{s,G}(\mu,\omega_{m_1},t)_{n=odd} + F_{s,G}(\mu,\omega_{m_1},t)_{n=even})$$

$$K_{\bar{w}_{G,ms,2}} = f_{s,G}(\mu,\omega_{m_2},t) + g_{s,G}(\mu,\omega_{m_2},t) + F_{s,G}(\mu,\omega_{m_2},t)_{n=odd} + F_{s,G}(\mu,\omega_{m_2},t)_{n=even})$$

$$K_{\bar{w}_{G,ms,3}} = f_{s,G}(\mu,\omega_{m_3},t) + g_{s,G}(\mu,\omega_{m_3},t) + F_{s,G}(\mu,\omega_{m_3},t)_{n=odd} + F_{s,G}(\mu,\omega_{m_3},t)_{n=even})$$

where

$$\theta_0 = (x^2+\mu^2/2)\theta_0 + x\mu\theta_{1s}$$

$$\theta_{1c} = (x^2+\mu^2/4)\theta_{1c}$$

$$\theta_{1s} = (x^2+3\mu^2/4)\theta_{1s} + 2x\mu\theta_0$$

$$\theta_{2c} = -(\mu^2\theta_0/2 + x\mu\theta_{1s})$$

$$\theta_{2s} = x\mu\theta_{1c}$$

$$\theta_{3c} = -\mu^2\theta_{1c}/4$$

$$\theta_{3s} = -\mu^2\theta_{1s}/4$$

$$\bar{w}_{G_{01}} = x(w_{G_0}/R\Omega)$$

$$\bar{w}_{G_{02}} = \mu(w_{G_0}/R\Omega)$$

$$\bar{w}_{Gcm_1} = x(w_{Gmc}/R\Omega)$$

$$\bar{w}_{Gs,m_1} = x(w_{Gms}/R\Omega)$$

$$\bar{w}_{Gc,m_2} = \bar{w}_{Gc,m_3} = \tfrac{1}{2}\mu(w_{Gmc}/R\Omega)$$

$$\bar{w}_{Gs,m_2} = -\bar{w}_{Gs,m_3} = \tfrac{1}{2}\mu(w_{Gms}/R\Omega)$$

$$\omega_{m_1} = \omega_m$$

$$\omega_{m_2} = \Omega+\omega_m$$

$$\omega_{m_3} = \Omega-\omega_m$$

$$x = r/R$$

$$\mu = V\cos i/R\Omega$$

$$\psi = \Omega t$$

$$(m = 1,2,3,\ldots)$$

$$f_c(\mu,\omega,t) = J_0(a_2k)F(k)\cos(\omega t - a_2k\cos\psi)$$

$$g_c(\mu,\omega,t) = J_0(a_2k)G(k)\sin(\omega t - a_2k\cos\psi)$$

$$F_c(\mu,\omega,t)_{n=odd} = \sum_{n=1,3,5,\ldots}'(-1)^{\frac{n-1}{2}}\Big[\frac{J_n(a_2k(n\frac{\Omega}{\omega}+1))}{n(\frac{\Omega}{\omega})+1} \times\{F(k(n\tfrac{\Omega}{\omega}+1))\sin(k(n\tfrac{\Omega}{\omega}+1)(a_1t-a_2\cos\psi)) + G(k(n\tfrac{\Omega}{\omega}+1))\cos(k(n\tfrac{\Omega}{\omega}+1)(a_1t-a_2\cos\psi))\} - \frac{J_n(a\,k(n\frac{\Omega}{\omega}-1))}{n(\frac{\Omega}{\omega})-1}\{F(k(n\tfrac{\Omega}{\omega}-1))\sin(k(n\tfrac{\Omega}{\omega}-1) \times(a_1t-a_2\cos\psi)) + G(k(n\tfrac{\Omega}{\omega}-1))\cos(k(n\tfrac{\Omega}{\omega}-1) \times(a_1t-a_2\cos\psi))\}\Big]$$

$$F_c(\mu,\omega,t)_{n=even} = \sum_{n=2,4,6,\ldots}'(-1)^{\frac{n}{2}}\Big[\frac{J_n(a_2k(n\frac{\Omega}{\omega}+1))}{n(\frac{\Omega}{\omega})+1} \times\{F(k(n\tfrac{\Omega}{\omega}+1))\cos(k(n\tfrac{\Omega}{\omega}+1)(a_1t-a_2\cos\psi)) - G(k(n\tfrac{\Omega}{\omega}+1))\sin(k(n\tfrac{\Omega}{\omega}+1)(a_1t-a_2\cos\psi))\} + \frac{J_n(a_2k(n\frac{\Omega}{\omega}-1))}{n(\frac{\Omega}{\omega})-1}\{F(k(n\tfrac{\Omega}{\omega}-1))\cos(k(n\tfrac{\Omega}{\omega}-1) \times(a_1t-a_2\cos\psi)) - G(k(n\tfrac{\Omega}{\omega}-1))\sin(k(n\tfrac{\Omega}{\omega}-1) \times(a_1t-a_2\cos\psi))\}\Big]$$

$$f_s(\mu,\omega,t) = J_0(a_2k)F(k)\sin(\omega t - a_2k\cos\psi)$$

$$g_s(\mu,\omega,t) = J_0(a_2k)G(k)\cos(\omega t - a_2k\cos\psi)$$

$$F_s(\mu,\omega,t)_{n=\text{odd}} = \sum_{n=1,3,5\ldots}{}' (-1)^{\frac{n-1}{2}}\Big[\frac{J_n(a_2k(n\frac{\Omega}{\omega}+1))}{n(\frac{\Omega}{\omega})+1}$$

$$\times\{F(k(n\tfrac{\Omega}{\omega}+1))\cos(k(n\tfrac{\Omega}{\omega}+1)(a_1t-a_2\cos\psi))$$

$$-G(k(n\tfrac{\Omega}{\omega}+1))\sin(k(n\tfrac{\Omega}{\omega}+1)(a_1t-a_2\cos\psi))$$

$$+\frac{J_n(a_2k(n\frac{\Omega}{\omega}-1))}{n(\frac{\Omega}{\omega})-1}\{F(k(n\tfrac{\Omega}{\omega}-1))\cos(k(n\tfrac{\Omega}{\omega}-1)$$

$$\times(a_1t-a_2\cos\psi))-G(k(n\tfrac{\Omega}{\omega}-1))\sin(k(n\tfrac{\Omega}{\omega}-1)$$

$$\times(a_1t-a_2\cos\psi))\}\Big]$$

$$F_s(\mu,\omega,t)_{n=\text{even}} = \sum_{n=2,4,6\ldots}{}' (-1)^{\frac{n}{2}}\Big[\frac{J_n(a_2k(n\frac{\Omega}{\omega}+1))}{n(\frac{\Omega}{\omega})+1}$$

$$\times\{F(k(n\tfrac{\Omega}{\omega}+1))\sin(k(n\tfrac{\Omega}{\omega}+1)(a_1t-a_2\cos\psi))$$

$$+G(k(n\tfrac{\Omega}{\omega}+1)\cos(k(n\tfrac{\Omega}{\omega}+1)(a_1t-a_2\cos\psi))\}$$

$$+\frac{J_n(a_2k(n\frac{\Omega}{\omega}-1))}{n(\frac{\Omega}{\omega})-1}\{F(k(n\tfrac{\Omega}{\omega}-1)\sin(k(n\tfrac{\Omega}{\omega}-1)$$

$$\times(a_1t-a_2\cos\psi))+G(k(n\tfrac{\Omega}{\omega}-1))\cos(k(n\tfrac{\Omega}{\omega}-1)$$

$$\times(a_1t-a_2\cos\psi))\}\Big]$$

$$f_{c,G}(\mu,\omega,t) = J_0(a_2k)F_G(k)\cos(\omega t-a_2k\cos\psi-k)$$

$$g_{c,G}(\mu,\omega,t) = J_0(a_2k)G_G(k)\sin(\omega t-a_2k\cos\psi-k)$$

$$F_{c,G}(\mu,\omega,t)_{n=\text{odd}} = \sum_{n=1,3,5\ldots}{}' (-1)^{\frac{n-1}{2}}\Big[\frac{J_n(a_2k(n\frac{\Omega}{\omega}+1))}{n(\frac{\Omega}{\omega})+1}$$

$$\times\{F_G(k(n\tfrac{\Omega}{\omega}+1))\sin(k(n\tfrac{\Omega}{\omega}+1)(a_1t-a_2\cos\psi-1))$$

$$+G_G(k(n\tfrac{\Omega}{\omega}+1))\cos(k(n\tfrac{\Omega}{\omega}+1)(a_1t-a_2\cos\psi-1))\}$$

$$-\frac{J_n(a_2k(n\frac{\Omega}{\omega}-1))}{n(\frac{\Omega}{\omega})-1}\{F_G(k(n\tfrac{\Omega}{\omega}-1))\sin(k(n\tfrac{\Omega}{\omega}-1)$$

$$\times(a_1t-a_2\cos\psi-1))+G_G(k(n\tfrac{\Omega}{\omega}-1))\cos(k(n\tfrac{\Omega}{\omega}-1)$$

$$\times(a_1t-a_2\cos\psi-1))\}\Big]$$

$$F_{c,G}(\mu,\omega,t)_{n=\text{even}} = \sum_{n=2,4,6\ldots}{}' (-1)^{\frac{n}{2}}\Big[\frac{J_n(a_2k(n\frac{\Omega}{\omega}+1))}{n(\frac{\Omega}{\omega})+1}$$

$$\times\{F_G(k(n\tfrac{\Omega}{\omega}+1))\cos(k(n\tfrac{\Omega}{\omega}+1)(a_1t-a_2\cos\psi-1))$$

$$-G_G(k(n\tfrac{\Omega}{\omega}+1))\sin(k(n\tfrac{\Omega}{\omega}+1)(a_1t-a_2\cos\psi-1))\}$$

$$+\frac{J_n(a_2k(n\frac{\Omega}{\omega}-1))}{n(\frac{\Omega}{\omega})-1}\{F_G(k(n\tfrac{\Omega}{\omega}-1))\cos(k(n\tfrac{\Omega}{\omega}-1)$$

$$\times(a_1t-a_2\cos\psi-1))-G_G(k(n\tfrac{\Omega}{\omega}-1))\sin(k(n\tfrac{\Omega}{\omega}-1)$$

$$\times(a_1t-a_2\cos\psi-1))\}\Big]$$

$$f_{s,G}(\mu,\omega,t) = J_0(a_2k)F_G(k)\sin(\omega t-a_2k\cos\psi-k)$$

$$g_{s,G}(\mu,\omega,t) = J_0(a_2k)G_G(k)\cos(\omega t-a_2k\cos\psi-k)$$

$$F_{s,G}(\mu,\omega,t)_{n=\text{odd}} = \sum_{n=1,3,5\ldots}{}' (-1)^{\frac{n-1}{2}}\Big[\frac{J_n(a_2k(n\frac{\Omega}{\omega}+1))}{n(\frac{\Omega}{\omega})+1}$$

$$\times\{F_G(k(n\tfrac{\Omega}{\omega}+1))\cos(k(n\tfrac{\Omega}{\omega}+1)(a_1t-a_2\cos\psi-1))$$

$$-G_G(k(n\tfrac{\Omega}{\omega}+1))\sin(k(n\tfrac{\Omega}{\omega}+1)(a_1t-a_2\cos\psi-1))\}$$

$$-\frac{J_n(a_2k(n\frac{\Omega}{\omega}-1))}{n(\frac{\Omega}{\omega})-1}F_G(k(n\tfrac{\Omega}{\omega}-1))\cos(k(n\tfrac{\Omega}{\omega}-1)$$

$$\times(a_1t-a_2\cos\psi-1))-G_G(k(n\tfrac{\Omega}{\omega}-1))\sin(k(n\tfrac{\Omega}{\omega}-1)$$

$$\times(a_1t-a_2\cos\psi-1))\}\Big]$$

$$F_{s,G}(\mu,\omega,t)_{n=\text{even}} = \sum_{n=2,4,6\ldots}{}' (-1)^{\frac{n}{2}}\Big[\frac{J_n(a_2k(n\frac{\Omega}{\omega}+1))}{n(\frac{\Omega}{\omega})+1}$$

$$\times\{F_G(k(n\tfrac{\Omega}{\omega}+1))\sin(k(n\tfrac{\Omega}{\omega}+1)(a_1t-a_2\cos\psi-1))$$

$$+G_G(k(n\tfrac{\Omega}{\omega}+1))\cos(k(n\tfrac{\Omega}{\omega}+1)(a_1t-a_2\cos\psi-1))\}$$

$$+\frac{J_n(a_2k(n\frac{\Omega}{\omega}-1))}{n(\frac{\Omega}{\omega})-1}\{F_G(k(n\tfrac{\Omega}{\omega}-1))\sin(k(n\tfrac{\Omega}{\omega}-1)$$

$$\times(a_1t-a_2\cos\psi-1))+G_G(k(n\tfrac{\Omega}{\omega}-1))\cos(k(n\tfrac{\Omega}{\omega}-1)$$

$$\times(a_1t-a_2\cos\psi-1))\}\Big]$$

and where

$a_1 = 2\pi R/c$

$a_2 = 2\mu R/c$

$k = \frac{\omega c}{2\pi Rx}$

$J_n(z)$: nth Bessel function of the first kind

$C(k) = F(k)+iG(k)$: Theodorsen function

$S(k) = F_G(k)+iG_G(k) = C(k)[J_0(k)-iJ_1(k)]+iJ_1(k)$

: Sears Function

Σ' means excluding the case that $n=N$ and $\omega=N\Omega$.

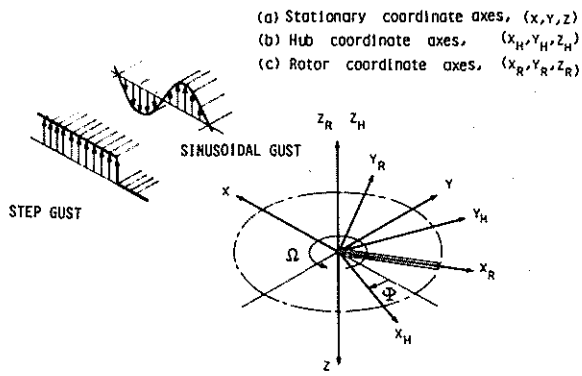

Figure 1. Gust shapes and the related coordinate systems.

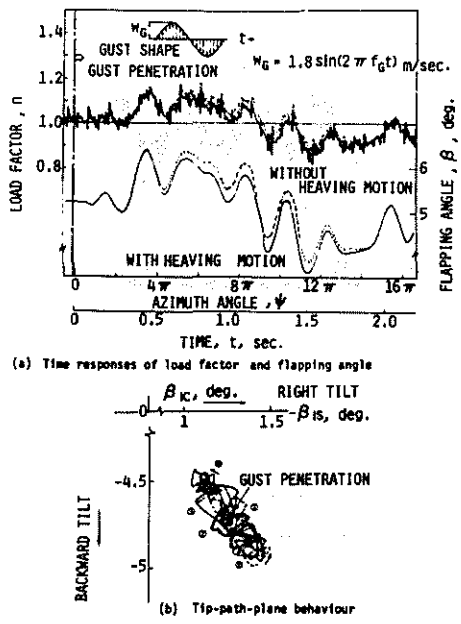

(a) Time responses of load factor and flapping angle

(b) Tip-path-plane behaviour

Figure 3. Rotor response due to a sinusoidal gust.

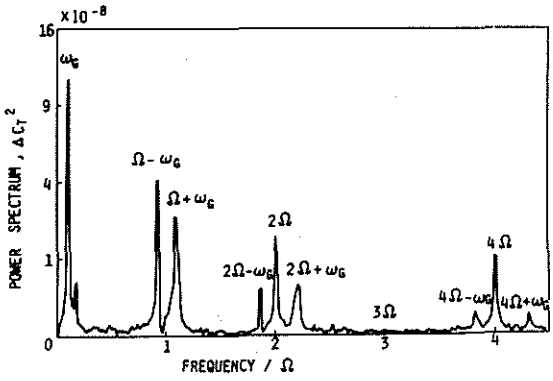

Figure 5. Power spectrum of the thrust.

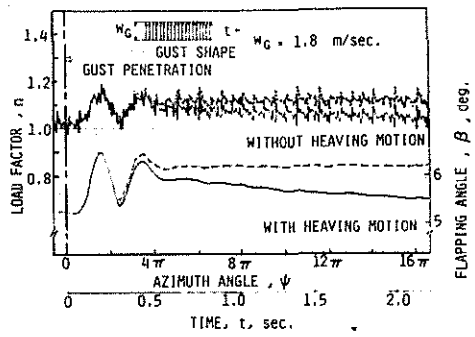

(a) Time responses of load factor and flapping angle

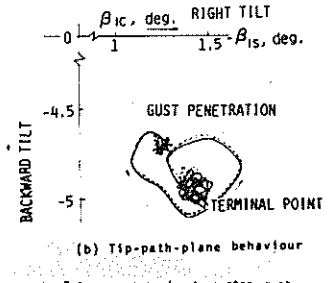

(b) Tip-path-plane behaviour

Figure 2. Rotor response due to a step gust.

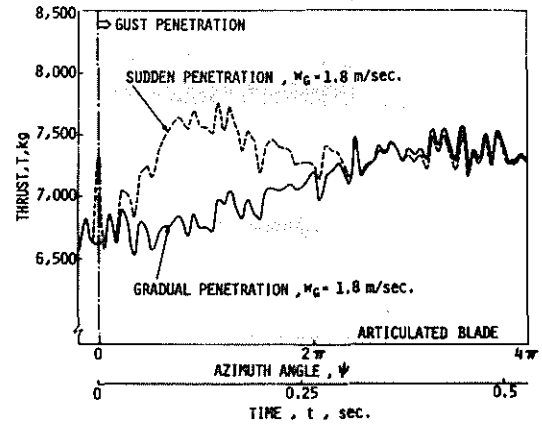

Figure 4. Difference in thrust responses between the sudden and the gradual penetrations of rotor into a step gust.

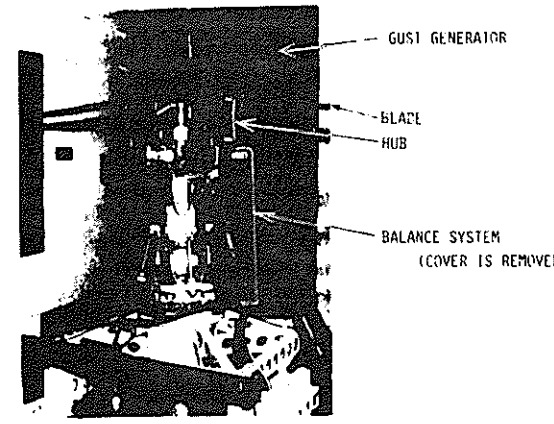

Figure 6. Rotor systems in gust tunnel.

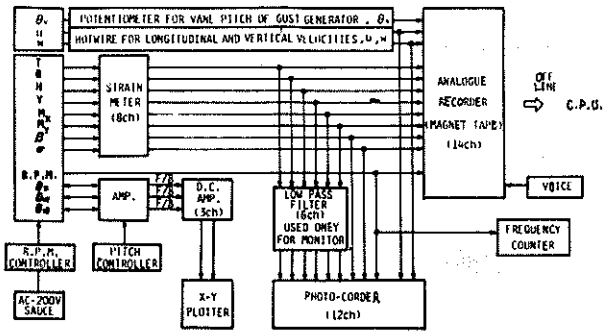

Figure 7. A systematic arrangement of the instruments, the rotor driving system and the filtering, monitoring and recording systems.

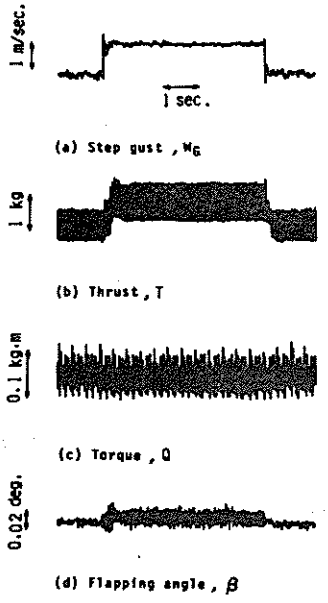

Figure 8. Gust responses in wind tunnel for a step gust.

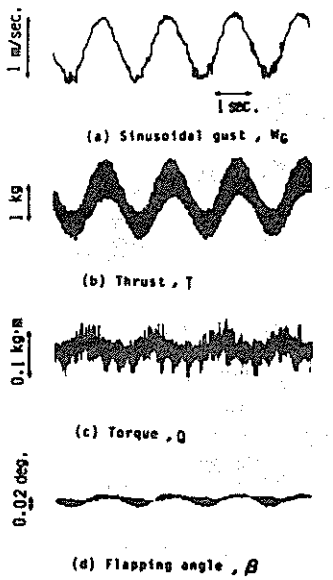

Figure 9. Gust responses in wind tunnel for a sinusoidal gust.

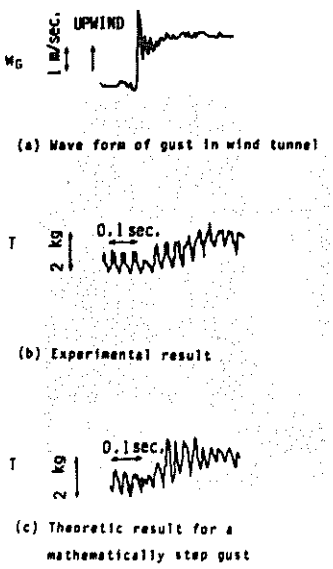

Figure 10. Comparison of the theoretical and experimental results of thrust response for a step gust.

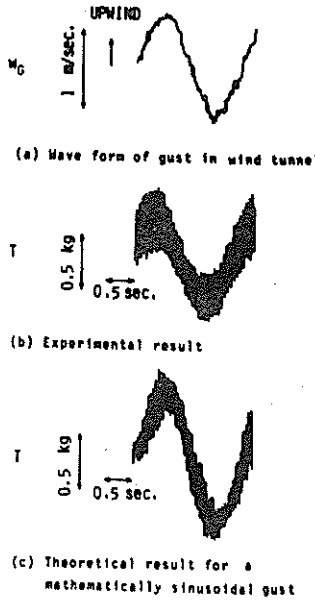

Figure 11. Comparison of the theoretical and experimental results of thrust response for a sinusoidal gust.

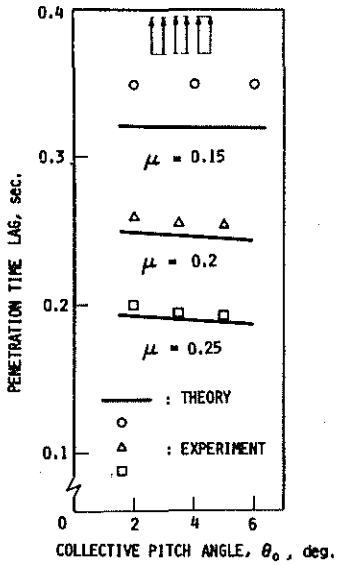

(a) Upwind

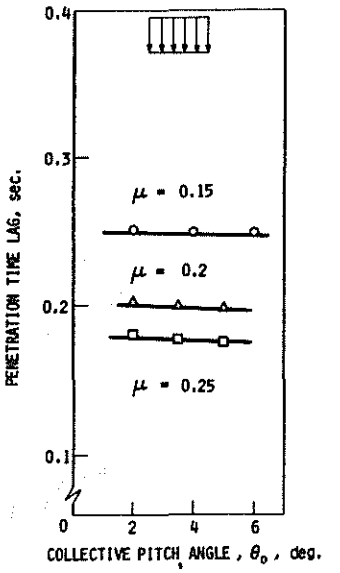

(b) Downwind

Figure 12. Time lag of the first peak of thrust response for a step gust.

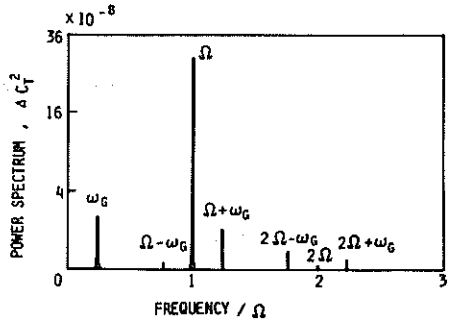

Figure 13. Power spectrum of the thrust response for a sinusoidal gust.

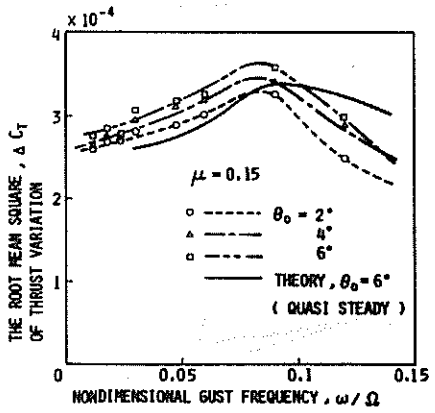

(a) Thrust

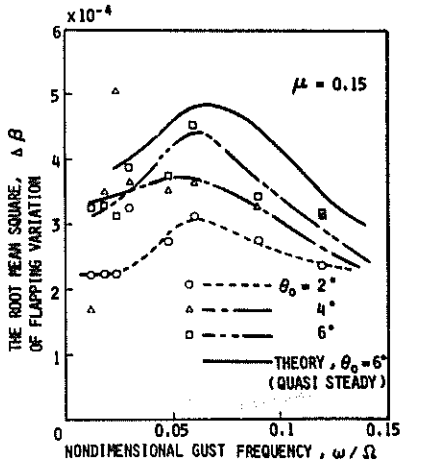

(b) Flapping angle

Figure 14. The deviation (root mean square) of the responses for sinusoidal gusts.

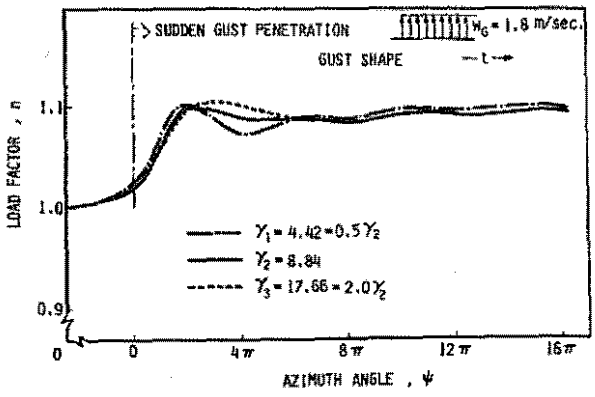

Figure 15. Effect of the Lock number on the load factor for sudden penetration into a step gust.

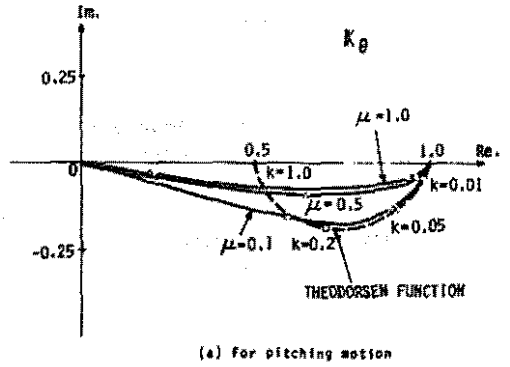

(a) For pitching motion

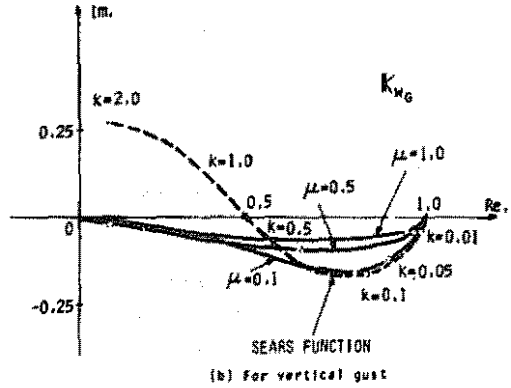

(b) For vertical gust

Figure 17. Lift deficiency functions.

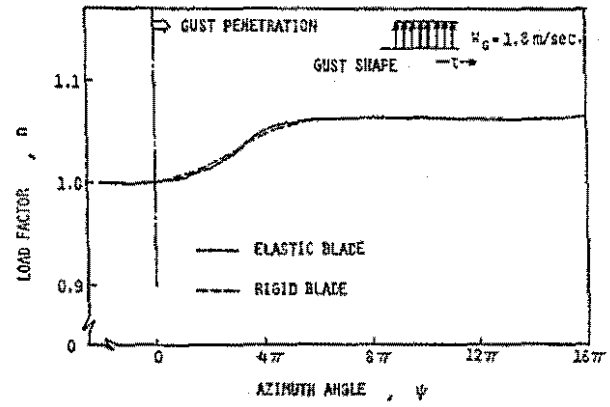

(a) For a step gust

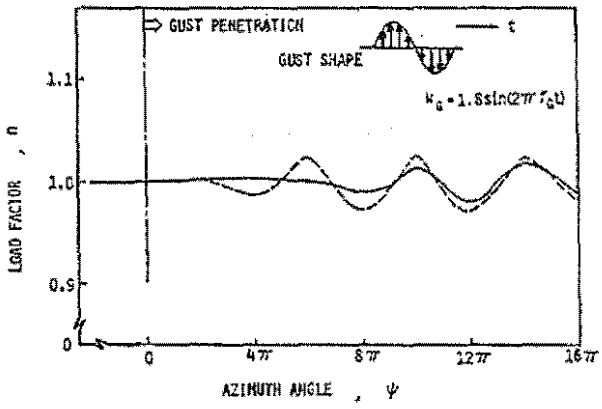

(b) For a sinusoidal gust

Figure 16. Effect of elasticity on the load factor.

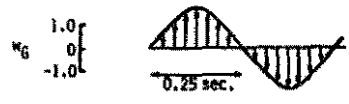

(a) A sinusoidal gust

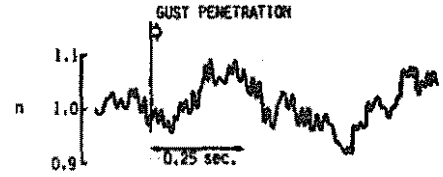

(b) Load factor based on unsteady aerodynamics

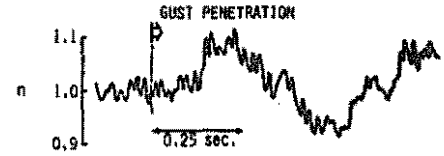

(c) Load factor based on quasi-steady aerodynamics

Figure 18. Effect of unsteady aerodynamics on the load factor for a sinusoidal gust.